Journal of Catalysis 268 (2009) 223–234

Contents lists available at ScienceDirect

Journal of Catalysis

journal homepage: www.elsevier.com/locate/jcat

Gold particle size effects in the gas-phase hydrogenation of *m*-dinitrobenzene over Au/TiO_2

Fernando Cárdenas-Lizana [a], Santiago Gómez-Quero [a], Hicham Idriss [b], Mark A. Keane [a,*]

[a] Chemical Engineering, School of Engineering and Physical Sciences, Heriot-Watt University, Edinburgh EH14 4AS, Scotland, United Kingdom
[b] Department of Chemistry, University of Aberdeen, Aberdeen AB24 3EU, Scotland, United Kingdom

ARTICLE INFO

Article history:
Received 31 August 2009
Revised 23 September 2009
Accepted 24 September 2009
Available online 28 October 2009

Keywords:
Au particle size
Au/TiO_2
Anatase
Rutile
m-Dinitrobenzene hydrogenation

ABSTRACT

The effect of Au particle size, supported on TiO_2, on the gas-phase hydrogenation of *m*-dinitrobenzene has been considered. The catalysts (Au loading = 0.1 and 1 mol%) were prepared by impregnation with $HAuCl_4$ and a range of Au particle sizes (3.4–10.0 nm) was generated by temperature-programmed reduction over the interval 603 K $\leqslant T \leqslant$ 1273 K. A thermal treatment of TiO_2 at $T \geqslant$ 873 K was required for the allotropic change from anatase to rutile but the presence of Au lowered the requisite temperature for complete transformation by up to 400 K. *m*-Dinitrobenzene hydrogenation exhibited a particle size sensitivity where higher specific rates were obtained with smaller Au particles, irrespective of the support composition (*i.e.* anatase:rutile ratio). The reaction over each Au/TiO_2 catalyst generated *m*-phenylenediamine (reduction of both $-NO_2$ groups) and/or *m*-nitroaniline (reduction of one $-NO_2$ group). A parallel/consecutive kinetic model has been applied to quantify the catalytic selectivity where Au particles <5 nm favoured *m*-nitroaniline production. The dependence of hydrogenation performance on Au particle size is accounted for in terms of a modification to Au electronic character, which impacts on *m*-dinitrobenzene adsorption/activation.

1. Introduction

Supported metal nanoparticles have found widespread use as catalysts in a range of industrial applications [1]. The term "structure sensitive" was first introduced in 1969 by Boudart [2], who proposed a dependence of the catalytic response on surface structure associated with variations in the exposed crystal plane(s) or changes in the metal crystallite size, typically over the range 1–10 nm. This is now a well-established effect on the hydrogenation of aromatic compounds over conventional transition metals (*e.g.* Pt [3] or Pd [4]). The development of gold catalysts is an emerging area of research that is attracting increasing attention [5] but has of yet limited applications in hydrogenation. This can be related to a lesser capacity of Au for hydrogen chemisorption due to the filled *d*-band and high associated ionization potential [6]. Nevertheless, when finely divided as small particles ($\leqslant$10 nm), gold is catalytically active in hydrogen-mediated reactions with some evidence of unique selectivities [7,8]. The reason for the selectivity response is still not well understood and there is no consensus regarding the Au size required to achieve an optimal specific hydrogenation rate. The results reported to date suggest that Au particles smaller than 5 nm (and especially those below 3 nm) are intrinsically more effective [9–11]. In the case of Au supported on TiO_2, an upward shift of the Fermi level has been observed for Au clusters of quantum size, *e.g.* the apparent Fermi level for Au/TiO_2 was determined to be −270 mV relative to NHE (Normal Hydrogen Electrode) for Au particles of 5 nm [12]. Higher hydrogenation activity for small Au particle size has been linked to enhanced H_2 dissociation on the corner and the edge positions [11,13]. Bus et al. [14], studying the liquid-phase hydrogenation of cinnamaldehyde to cinnamyl alcohol over Au/Al_2O_3, attributed the highest activity recorded to a more effective C=O activation over small (<2 nm) Au clusters. Mohr et al. [15] have identified the edge sites of gold nanoparticles (in Au/TiO_2 and Au/ZrO_2) as the preferred sites for C=O activation in the hydrogenation of acrolein to allyl alcohol. It should, however, be noted that a decrease in hydrogenation activity has also been observed for Au particles <2 nm, which has been linked to a loss of metallic character [9,16]. There is some limited evidence that hydrogenation selectivity (in the treatment of but-2-enal) can also be influenced by variations in Au dispersion [17] but such an effect has yet to be irrefutably established. The ultimate Au particle size is determined by the Au precursor [18,19], preparation method [20,21], activation conditions [22–24] and the nature of the support [25,26], which in turn can influence hydrogenation performance to varying degrees. It is difficult to establish an explicit link between catalytic performance and Au particle size from the available literature.

* Corresponding author.
E-mail address: M.A.Keane@hw.ac.uk (M.A. Keane).

0021-9517/$ - see front matter © 2009 Elsevier Inc. All rights reserved.
doi:10.1016/j.jcat.2009.09.020

Aromatic amino-compounds are extensively used as intermediates in the production of a diversity of fine chemicals [1]. The traditional manufacture route, from the corresponding nitro-derivate using stoichiometric amounts of iron as reducing agent in acid media (Béchamp process), is no longer viewed as sustainable due to the production of large quantities of toxic iron oxides [27]. An alternative batch liquid-phase operation over supported Pt [28] or Pd [29] also has an associated negative environmental impact due to the formation of secondary harmful products, *i.e.* azo- [30] and/or azoxy-derivates [31]. Recently, there have been studies [32–35] that have shown the potential of Au for chemoselective $-NO_2$ group reduction in batch liquid-phase operation. We have demonstrated exclusivity in the gas-phase continuous hydrogenation of a range of nitroarenes over supported gold-based catalysts [9,21,25,36,37]. In this report, we extend that work and provide for the first time a direct correlation between catalytic response and Au particle size in the hydrogenation of *m*-dinitrobenzene (*m*-DNB) over Au/TiO_2. Moreover, we demonstrate that product composition can be altered (or tuned) by varying Au particle size.

2. Experimental

2.1. Materials and catalyst preparation

The TiO_2 (Degussa, P25) support was used as received. Two (0.1 and 1 mol%) supported Au catalysts were prepared by standard impregnation of the TiO_2 support (5 g) with $HAuCl_4$ (Aldrich, 25×10^{-3} g cm^{-3}, pH 2) solutions. The slurry was heated (2 K min^{-1}) to 353 K and maintained under constant agitation (600 rpm) in an ultra pure He purge (>99.99%, BOC). The solid residue was dried in a flow of He at 383 K for 3 h, sieved into a batch of 75 μm average diameter and stored under He in the dark at 277 K. Prior to use in catalysis, the samples were activated in 60 cm^3 min^{-1} H_2 at 2 K min^{-1} to a final temperature in the range 603–873 K, which was maintained for at least 1 h. For comparison purposes, a series of rutile-supported Au catalysts were prepared using two approaches: (i) activation of 0.1 mol% and 1 mol% Au/TiO_2 in H_2 to 1273 K; and (ii) formation of rutile (confirmed by XRD analysis) by thermal treatment of TiO_2 to 1273 K and subsequent impregnation with $HAuCl_4$ (0.1 mol% Au), post-treatment as mentioned above. After activation, the samples were passivated in 1% v/v O_2/He at 298 K for off-line analysis.

2.2. Characterization analyses

BET area and H_2 chemisorption were recorded using the commercial CHEMBET 3000 (Quantachrome Instrument) unit. The samples were loaded into a U-shaped Quartz cell (100 mm × 3.76 mm i.d.) and heated in 17 cm^3 min^{-1} (Brooks mass flow controlled) 5% v/v H_2/N_2 to the final reduction temperature ($603 \leqslant T \leqslant 1273$ K) at 2 K min^{-1}. The effluent gas was passed through a liquid N_2 trap and the changes in H_2 consumption were monitored by TCD with data acquisition/manipulation using the TPR Win™ software. The reduced samples were swept with 65 cm^3 min^{-1} N_2 for 1.5 h, cooled to room temperature and subjected to H_2 chemisorption using a pulse (10–50 μl) titration procedure. Hydrogen pulse introduction was repeated until the signal area was constant, indicating surface saturation. BET areas were recorded with a 30% v/v N_2/He flow; pure N_2 (99.9%) served as the internal standard. At least two cycles of N_2 adsorption–desorption in the flow mode were used to determine the total surface area using the standard single-point method. BET surface area and H_2 uptake values were reproducible to within ±5%; the values quoted in this paper are the mean.

Powder X-ray diffractograms were recorded on a Bruker/Siemens D500 incident X-ray diffractometer using Cu Kα radiation. The samples were scanned at a rate of 0.02° step^{-1} over the range $20° \leqslant 2\theta \leqslant 90°$ (scan time = 5 s step^{-1}). Diffractograms were identified using the JCPDS-ICDD reference standards, *i.e.* anatase (21-1272), rutile (21-1276) and Au (04-0784). The rutile:anatase ratios were determined by XRD according to the method described by Fu et al. [38], *i.e.*

$$\%\ \text{Rutile} = \frac{1}{[(A/R) \times 0.884 + 1]} \times 100 \tag{1}$$

where A and R represent the peak areas associated with the main reflections for anatase ($2\theta = 25.3°$) and rutile ($2\theta = 27.4°$), respectively. Diffuse reflectance UV–vis (DRS UV–vis) measurements were conducted using a Perkin–Elmer Lambda 35 UV–vis spectrometer with $BaSO_4$ powder as reference; absorption profiles were calculated from the reflectance data using the Kubelka–Munk function. Transmission electron microscopy analysis employed a JEOL JEM 2011 HRTEM unit with a UTW energy dispersive X-ray detector (EDX) detector (Oxford Instruments) operated at an accelerating voltage of 200 kV and using Gatan DigitalMicrograph 3.4 for data acquisition/manipulation. The samples for analysis were prepared by dispersion in acetone and deposited on a holey carbon/Cu grid (300 Mesh). Up to 600 individual metal particles were counted for each catalyst and the surface area-weighted mean Au diameter (d_p) was calculated from

$$d_p = \frac{\sum_i n_i d_i^3}{\sum_i n_i d_i^2} \tag{2}$$

where n_i is the number of particles of diameter d_i. The size limit for the detection of gold particles on TiO_2 is *ca.* 1 nm.

2.3. Catalytic procedure

The reactions were carried out under atmospheric pressure, *in situ* immediately after activation, in a fixed bed vertical continuous flow glass reactor ($l = 600$ mm, i.d. = 15 mm) at $T = 473$ K. The catalytic reactor and operating conditions to ensure negligible heat/mass transport limitations have been fully described elsewhere [39] but some features, pertinent to this study, are given below. A preheating zone (layer of borosilicate glass beads) ensured that the organic reactant was vapourized and reached the reaction temperature before contacting the catalyst. Isothermal conditions (±1 K) were maintained by thoroughly mixing the catalyst with ground glass (75 μm). The temperature was continuously monitored by a thermocouple inserted in a thermowell within the catalyst bed. A butanolic solution of *m*-DNB reactant was delivered, in a co-current flow of H_2, *via* a glass/teflon air-tight syringe and a teflon line, using a microprocessor-controlled infusion pump (Model 100 kd Scientific) at a fixed calibrated flow rate. The inlet $-NO_2$ molar flow (F_{-NO_2}) was in the range 0.08–0.20 mmol_{-NO_2} h^{-1} where the molar metal to inlet molar $-NO_2$ feed rate ratio spanned a 6×10^{-4}–629×10^{-4} h^{-1} interval. Hydrogen content in the feed was at least 100 times in excess of the stoichiometric requirement, the flow rate of which was monitored using a Humonics (Model 520) digital flowmeter; $GHSV = 2 \times 10^4$ h^{-1}. In a series of blank tests, the passage of *m*-DNB reactant in a stream of H_2 through the empty reactor or over the support alone, *i.e.* in the absence of Au, did not result in any detectable conversion. The reactor effluent was frozen in a liquid nitrogen trap for subsequent analysis, which was made using a Perkin–Elmer Auto System XL gas chromatograph equipped with a programmed split/splitless injector and a flame ionization detector, employing a DB-1 50 m × 0.20 mm i.d., 0.33 μm film thickness capillary column (J&W Scientific), as described elsewhere [40]. *m*-DNB (Aldrich,

⩾98%) and 1-butanol (Riedel-de Haën) were used as supplied without further purification. Hydrogenation activity is expressed in terms of the degree of nitro-group reduction (x_{-NO_2})

$$x_{-NO_2} = \frac{[-NH_2]_{out}}{[-NO_2]_{in}} = \frac{2 \times [m\text{-PDM}]_{out} + [m\text{-NAN}]_{out}}{2 \times [m\text{-DNB}]_{in}} \quad (3)$$

where [*m*-NAN] and [*m*-PDM] are, respectively, the concentrations of *m*-nitroaniline and *m*-phenylenediamine, and the subscripts *in* and *out* refer to the inlet and outlet streams. Catalyst activity is also quantified in terms of the fractional conversion of *m*-DNB ($x_{m\text{-DNB}}$)

$$x_{m\text{-DNB}} = \frac{[m\text{-DNB}]_{in} - [m\text{-DNB}]_{out}}{[m\text{-DNB}]_{in}} \quad (4)$$

while selectivity in terms of (say) *m*-NAN ($S_{m\text{-NAN}}$) is given by

$$S_{m\text{-NAN}} = \frac{[m\text{-NAN}]_{out}}{[m\text{-DNB}]_{in} - [m\text{-DNB}]_{out}} \quad (5)$$

3. Results and discussion

The sample notation for the Au/TiO_2 catalysts, Au loading and activation conditions, H_2 chemisorption, DRS UV–vis results, rutile content and BET surface area are given in Table 1, along with the mean Au particle sizes (and range of values) obtained from TEM analysis. Titanium dioxide crystallizes primarily in three different forms, *i.e.* anatase, rutile and brookite. Anatase and rutile have found widespread use in catalytic applications [41]. In both structures, the basic building block consists of a titanium atom surrounded by six oxygens in an octahedral configuration, where structural difference arises from the packing of these octahedra [41]. Anatase is the thermodynamically unstable crystal form [42] and anatase→rutile phase conversion is possible at $T > 973$ K [43,44]. Heat treatment in H_2 can induce (i) the condensation of surface hydroxyl groups [43] and (ii) the removal of the bridging oxygen shared by the Ti atoms [44] with subsequent water desorption and the formation of surface defects that quickly expand to the bulk [45,46] leading to rutile formation.

3.1. Catalyst characterization

3.1.1. H_2 chemisorption/DRS UV–vis

We have reported previously [25] the TPR profile for Au/TiO_2 prepared by impregnation and established that the precursor was reduced to zero valent Au at 603 K, as has also been demonstrated elsewhere [47]. The aim of this study is to address the possible effects of Au size in determining the activity and the selectivity in the

Table 1
Gold loading and activation temperature with associated H_2 chemisorption values, DRS UV–vis characteristics, TEM-derived mean Au particle size (d_p), specific surface area (S_{Au}), % fraction of rutile, BET surface area and pseudo-first order rate constants for nitro-group reduction in the hydrogenation of *m*-DNB over Au/TiO_2.

Catalyst	Au content (mol%)	Activation temperature (K)	H_2 uptake (μmol g_{Au}^{-1})	DRS UV–vis A_{max} (nm)	d_p (nm)	S_{Au}[a] (m^2 g_{Au}^{-1})	% Rutile[b]	BET (m^2 g^{-1})	$10 \times k$ (h^{-1})
Au/TiO_2-1	0.1	603	162	510	3.4	93	16	49	920
Au/TiO_2-2	0.1	873	109	560	4.7	68	67	28	300
Au/TiO_2-3	1	603	15	570	6.1	52	20	47	60
Au/TiO_2-4	1	873	4	600	9.4	34	94	20	2

[a] $S_{Au} = 6/(\rho_{Au} \times d_p)$ where $\rho_{Au} = 18.88$ g cm^{-3}.
[b] Based on XRD analysis (see Eq. (1)).

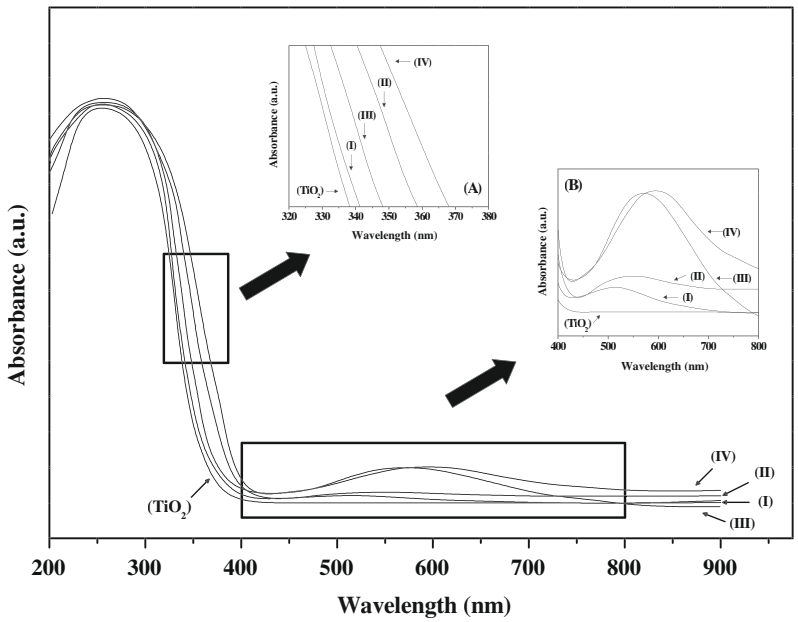

Fig. 1. DRS UV–vis spectra of starting TiO_2 support and passivated/reduced (I) Au/TiO_2-1, (II) Au/TiO_2-2, (III) Au/TiO_2-3 and (IV) Au/TiO_2-4. Inset: DRS spectra magnifications in the (A) UV and (B) visible regions.

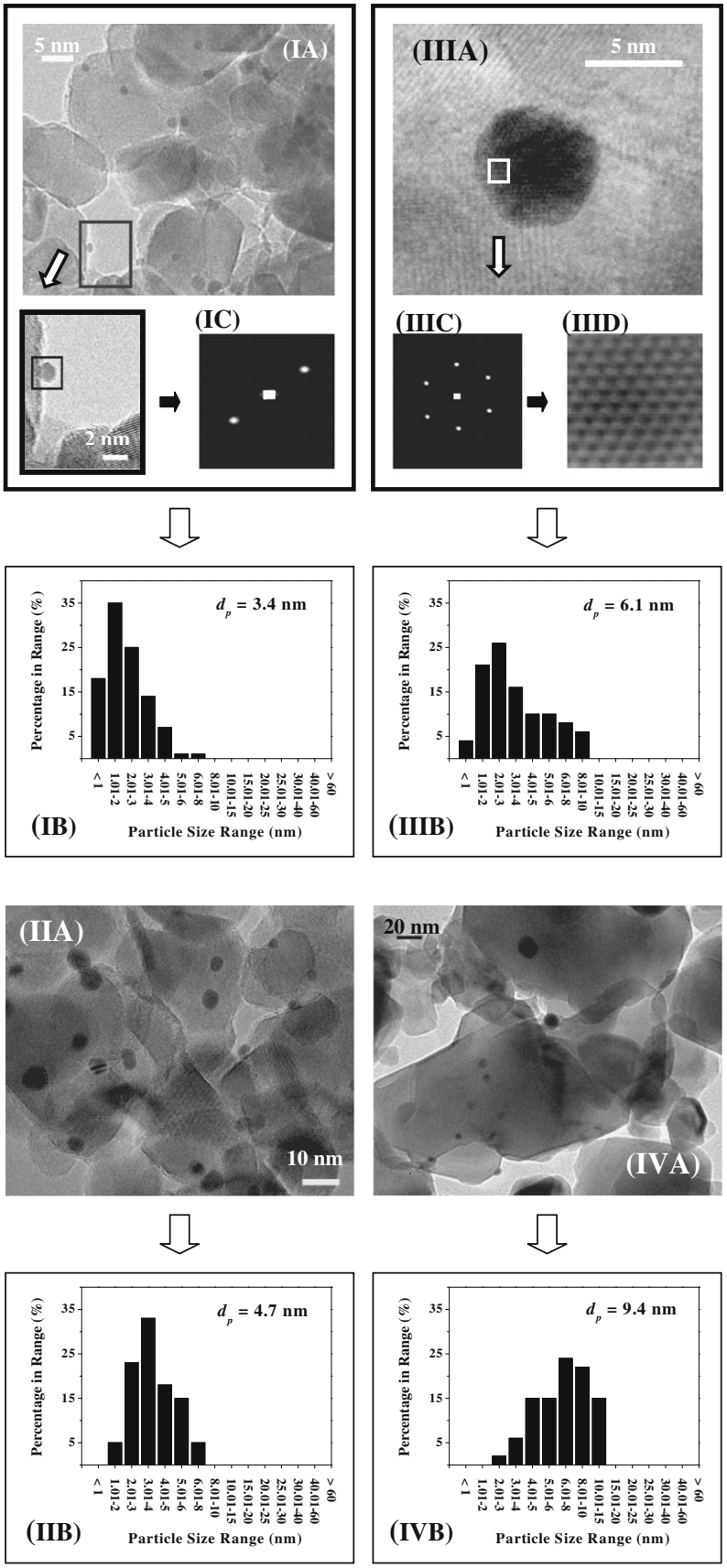

Fig. 2. Representative (A) TEM images, (B) Au particle size distributions and (C) diffractogram patterns associated with selected areas of passivated/reduced (I) Au/TiO_2-1, (II) Au/TiO_2-2, (III) Au/TiO_2-3 and (IV) Au/TiO_2-4. *Note*: Inverse fast Fourier transform (IFFT) for framed section in IIIA (Au/TiO_2-3) is shown in image (IIID).

hydrogenation of *m*-DNB. In order to modify Au dispersion, two approaches have been taken, *i.e.* variation of (a) Au loading (0.1 and 1 mol%) and (b) activation temperatures (603–1273 K). Both factors have been shown [23,48] to impact on Au particle size. Hydrogen uptake (at ambient temperature) on all the Au/TiO_2 samples ($\leqslant$162 μmol g_{Au}^{-1}) was significantly lower than that quoted in the literature for conventional supported transition metal catalysts with a similar metal content, *e.g.* Pd/Al_2O_3 (1870 μmol g_{Pd}^{-1}) [49] and Pt/SiO_2 (1461 μmol g_{Pt}^{-1}) [13]. This is consistent with a low capacity of Au for H_2 chemisorption due to the high energy barrier for H_2 dissociation on group IB metals [50]. Nevertheless, the specific uptake was measurably lower on samples with a higher Au content (*e.g.* Au/TiO_2-3 *vs.* Au/TiO_2-1). It has been reported [22,51] that an increase in Au content facilitates agglomeration and the formation of larger Au particles. Moreover, a consensus has emerged from the literature [13,52,53] that H_2 uptake is higher on smaller Au particles with a greater preponderance of defects. Our observed variations in H_2 uptake suggest differences in Au dispersion with varying Au content and activation temperature.

The DRS UV–vis spectra recorded for the support and the Au/TiO_2 catalysts are presented in Fig. 1, where selected areas in the UV (320–380 nm) and visible (400–800 nm) regions have been magnified and are shown as insets (A) and (B), respectively. All the samples absorb in the UV range as expected for TiO_2 where the Au/TiO_2 samples (profiles I–IV) exhibit a displacement of up to *ca.* 30 nm in the UV band to higher wavelengths. This response has been associated elsewhere [54] with the formation of rutile. In the visible region (B), the spectrum for the starting TiO_2 support is featureless, as observed previously [25,55]. In contrast, the profiles for the activated catalysts exhibit a band with a peak maximum in the range 500–600 nm (see Table 1). This response is qualitatively consistent with the presence of Au nanoparticles supported on titania [56]. There is a distinct shift in peak maximum to longer wavelengths with increasing Au loading and/or activation temperature. Similar shifts have been reported in the literature and attributed to a decrease in Au dispersion [57,58].

3.1.2. TEM/particle size distribution

Representative TEM images (A) and Au particle size distributions (B) associated with Au/TiO_2-1 (I), Au/TiO_2-2 (II), Au/TiO_2-3 (III) and Au/TiO_2-4 (IV) are given in Fig. 2. The TEM images reveal a pseudo-spherical morphology for the Au particles in all the samples, suggesting a relatively weak interaction and a small area of contact at the interface between the metal crystallites and the TiO_2 support. This is in agreement with the published literature [59] where Au/TiO_2 prepared by impregnation is characterized by a metal-support contact angle >90°. The *d*-spacings (0.23/0.20) between the planes in the atomic lattice obtained from the diffractogram patterns (C) of individual Au particles associated with Au/TiO_2-1 (I) and Au/TiO_2-3 (III) are consistent with the (1 1 1) and

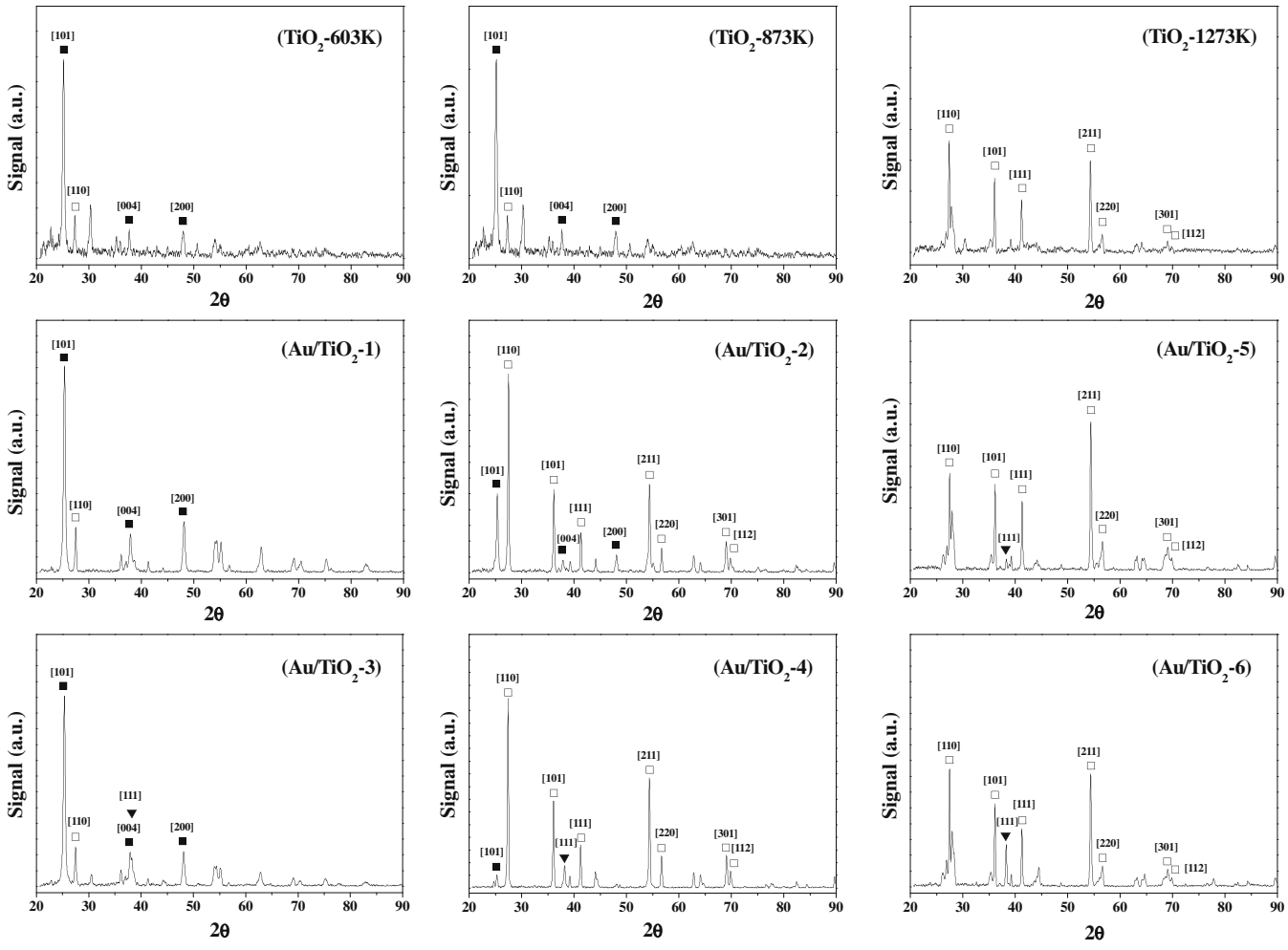

Fig. 3. XRD patterns for the TiO_2 support post-thermal treatment (from 603 K to 1273 K) and passivated/reduced Au/TiO_2 catalysts. *Note*: Peak assignments based on JCPDS-ICDD reference data: (■) anatase (21-1272); (□) rutile (21-1276); (▼) Au (04-0784).

(2 0 0) planes of metallic gold (JCPDS-ICDD 04-0784) and further corroborate the reduction of the precursor to zero valent Au post-activation at 603 K. In order to analyze the distribution of Au atoms in more detail, an IFFT (inverse fast Fourier transform) was applied. The transformed image (IIID) corresponding to the selected region in IIIA shows the arrangement of Au atoms in the crystal structure.

An increase in Au particle size with increasing metal content and/or activation temperature is demonstrated by the TEM-generated size histograms shown in Fig. 2. The catalysts which bear larger mean particle sizes (Au/TiO_2-3 and Au/TiO_2-4 shown in IIIB and IVB, respectively) present a wider size distribution when compared with Au/TiO_2-1 and Au/TiO_2-2. The surface area-weighted mean Au sizes fell within the range of 3.4 nm (Au/TiO_2-1) and 9.4 nm (Au/TiO_2-4). A gold particle size $\leqslant$5 nm has been suggested as critical for catalytic activity in hydrogen-mediated processes [7,11]; % of particles $\leqslant$5 nm decreases in the sequence Au/TiO_2-1 (95%) > Au/TiO_2-2 and Au/TiO_2-3 (75%) > Au/TiO_2-4 (25%). It is worth flagging that the majority (85%) of the Au particles in Au/TiO_2-4, with higher Au content and activated at an elevated temperature (873 K), exhibited particle diameters $\leqslant$10 nm. It should also be noted that the samples exhibited a colour change from the starting white powder to purple and ultimately to black during the thermal treatment. Colour changes have been associated with a partial reduction of TiO_2 [60], and variations in colouration correlate with the number of bulk defects. One consequence of this change in appearance is an increase in rutile content [61], which is suggested by our DRS UV–vis measurements.

3.1.3. XRD/BET

Powder XRD patterns of the TiO_2 support post-thermal treatment along with those for Au/TiO_2-1, Au/TiO_2-2, Au/TiO_2-3 and Au/TiO_2-4 are presented in Fig. 3. In order to confirm the bulk composition for each sample, the XRD patterns were compared with the JCPDS-ICDD standards for anatase (21-1272), rutile (21-1276) and Au (04-0784). The diffractograms for TiO_2 activated at 603 K and 873 K are essentially equivalent, exhibiting peaks at 25.3°, 37.8° and 48.1° that are consistent with the (1 0 1), (0 0 4) and (2 0 0) planes associated with tetragonal anatase. In addition, a signal at 27.4° is observed corresponding to the (1 1 0) main plane of tetragonal rutile. This XRD response is consistent with a mixture of anatase and rutile forms of TiO_2 where anatase:rutile $\approx$ 5:1, which is characteristic of Degussa P25 [62] for thermal treatment up to 923 K [44]. The diffractograms for Au/TiO_2-1 and Au/TiO_2-2 (Au loading = 0.1 mol%) do not present any detectable peak associated with Au, *i.e.* the metal particles are below the detection limits (<3–5 nm [63,64]), which is consistent with the TEM analysis. In contrast, the catalysts with higher Au content exhibited a peak at $2\theta = 38.1°$ that corresponds to the (1 1 1) Au plane. A stronger XRD reflection is evident at higher activation temperature (Au/TiO_2-4), indicative of Au sintering as demonstrated by TEM analysis (Fig. 2).

The XRD diffractograms for Au/TiO_2-1 and Au/TiO_2-3 (reduced at 603 K) exhibit the same XRD signals due to the support as observed for the starting TiO_2. In contrast, the XRD pattern for Au/TiO_2-2 (reduced at 873 K) shows, in addition, new signals at 36.1°, 41.2°, 54.3°, 56.6°, 69.0° and 69.8° corresponding to the

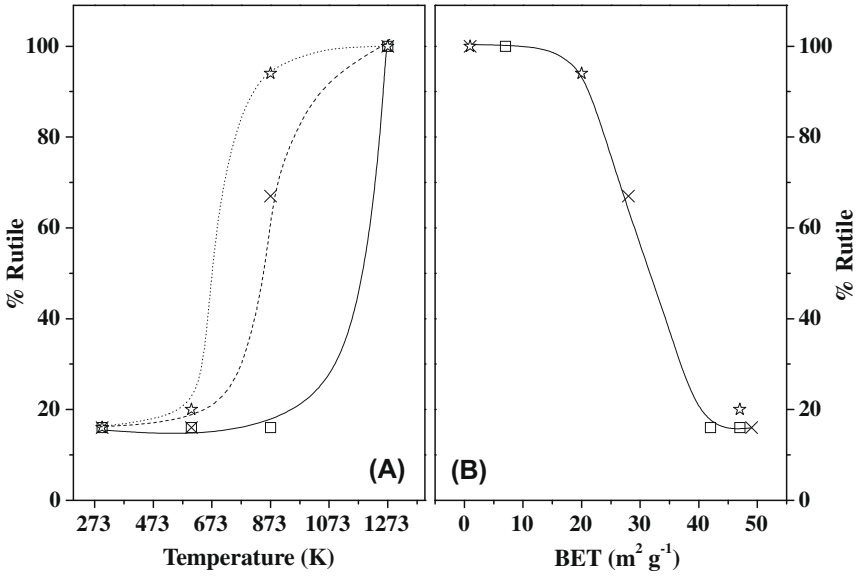

Fig. 4. Variations in rutile content with (A) activation temperature and (B) BET surface area for (□) TiO_2 and Au/TiO_2 with (×) 0.1 and (☆) 1 mol% Au loading.

Table 2
Gold loading with activation temperature and associated H_2 chemisorption values, TEM-derived mean Au particle size (d_p), specific surface area (S_{Au}), BET surface area and pseudo-first order rate constants for nitro-group reduction in the hydrogenation of *m*-DNB over Au/rutile.

Catalyst	Au content (mol%)	Activation temperature (K)	H_2 uptake (μmol g_{Au}^{-1})	d_p (nm)	S_{Au}[a] ($m^2\ g_{Au}^{-1}$)	BET ($m^2\ g^{-1}$)	$10^3 \times k\ (h^{-1})$
Au/TiO_2-5	0.1	1273	12	7.0	45	1	11
Au/TiO_2-6	1	1273	4	10.0	32	1	1
Au/TiO_2-7	0.1	603	66	6.4	50	1	37
Au/TiO_2-8	0.1	873	23	8.8	36	1	20

[a] $S_{Au} = 6/(\rho_{Au} \times d_p)$ where $\rho_{Au} = 18.88\ g\ cm^{-3}$.

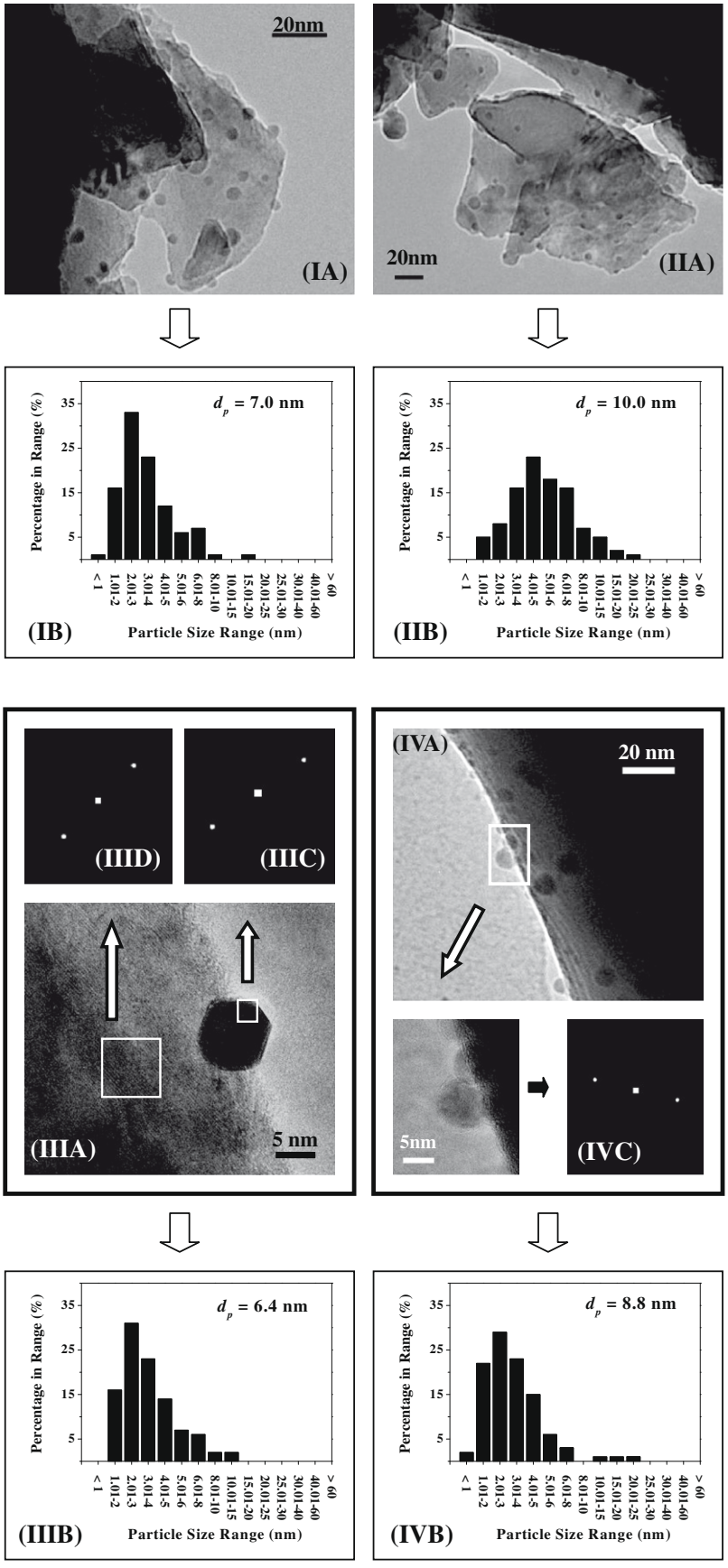

Fig. 5. Representative (A) TEM images, (B) Au particle size distributions and diffractogram patterns associated with (C) isolated Au particles and (D) support for passivated/reduced (I) Au/TiO_2-5, (II) Au/TiO_2-6, (III) Au/TiO_2-7 and (IV) Au/TiO_2-8.

(1 0 1), (1 1 1), (2 1 1), (2 2 0), (3 0 1) and (1 1 2) planes of rutile. Furthermore, it should be noted that the relative intensity of the two main peaks for anatase and rutile at $2\theta = 25.3°$ (1 0 1) and 27.4° (1 1 0), respectively (*ca.* 1:3) differs from that which characterizes the starting TiO_2 support (*ca.* 5:1) taken to the same temperature (873 K). This result suggests that the presence of Au facilitated the transition of anatase to rutile during the reduction of Au/TiO_2-2. This response also applies to Au/TiO_2-4, *i.e.* same activation temperature but increased Au loading, where stronger rutile XRD reflections and a decrease in the anatase:rutile ratio (*ca.* 1:20) are in evidence. Indeed, only the main peak for anatase (at $2\theta = 25.3°$) is distinguishable: an increase in Au loading favoured the anatase→rutile transformation. The requisite temperature for TiO_2 phase transformation can be affected by the inclusion of a range of additives [65,66] that catalyze or inhibit the transformation. Vargas et al. [66] reported that the incorporation of alkali metal, alkaline earth metal and group 3 and 13 elements modified the requirements for the TiO_2 phase transformation (by more than 330 K) where a linear relationship between the anatase-rutile transition temperature and the ionic radius of the additive was established. While the incorporation of Cu [67], Th [67] and Fe [67,68] has been reported to favour a TiO_2 allotropic transformation, the opposite effect has been shown in the case of Au [69,70]. Our findings suggest that the presence of Au lowers the temperature requirements for rutile formation, where Au content is a critical factor. This is illustrated in Fig. 4 where the rutile content, obtained from XRD analysis (see Eq. (1)), is plotted as a function of activation temperature (A) and BET surface area (B). It can be seen that the rutile content in the starting TiO_2 and Au-loaded TiO_2 essentially coincides for thermal treatment at $T \leqslant 603$ K whereas phase transformation is dramatically promoted by the incorporation of Au at $T > 603$ K. A switch from anatase to rutile is accompanied by a decrease in surface area, as noted elsewhere [71] and shown in Fig. 4B. A complete transformation to the rutile phase upon treatment at 1273 K was a feature of TiO_2 with and without Au inclusion. This is in line with the literature [44] where for pure (undoped) TiO_2, the transition of the thermodynamically unstable anatase (to rutile) at $T > 973$ K has been established.

The reduced state of TiO_2 has been found to markedly affect the size, shape and electronic character of supported Au nanoparticles [72,73]. Changes to such structural features can influence the catalytic properties of Au in hydrogenation reactions [9,16,25]. The possible effect on the catalytic response due to the differences in the anatase:rutile ratio and/or Au-support interactions was investigated by preparing a series of rutile-supported Au catalysts. In order to generate a range of Au particle sizes, two approaches were taken (see Section 2) (i) activation in H_2 of 0.1 mol% (Au/TiO_2-5) and 1 mol% (Au/TiO_2-6) loadings at 1273 K and (ii) preparation of rutile by thermal treatment of TiO_2 to 1273 K (see Fig. 3, TiO_2-1273 K) and subsequent impregnation with $HAuCl_4$ followed by activation at 603 K (Au/TiO_2-7) or 873 K (Au/TiO_2-8). The critical characterization results for these samples are compiled in Table 2. The XRD diffractogram patterns for Au/TiO_2-5 and Au/TiO_2-6, shown in Fig. 3, demonstrate the presence of rutile and metallic Au with no evidence of the anatase phase. Representative TEM images (A) and Au particle size distributions (B) of Au/TiO_2-5 (I), Au/TiO_2-6 (II), Au/TiO_2-7 (III) and Au/TiO_2-8 (IV) are shown in Fig. 5. The diffractogram pattern for an isolated Au particle and the support are shown in images IIIC/IVC and IIID, respectively. The *d*-spacings (0.20 and 0.33) confirm the presence of metallic gold and rutile. In addition to anatase→rutile conversion, activation at 1273 K resulted in Au sintering. At a common reduction temperature, Au/rutile catalyst exhibited a broader Au size distribution (and larger mean values) than that observed for Au/anatase, *i.e.* Au/TiO_2-1 *vs.* Au/TiO_2-7 and Au/TiO_2-2 *vs.* Au/TiO_2-8 (see Tables 1 and 2). This response suggests a Au size dependency on the allotropic form of the TiO_2 support and is in line with related studies where a weaker interaction (leading to metal agglomeration) with rutile relative to anatase has been proposed for Pd [74] and Ni [75].

3.2. Catalytic activity/selectivity

3.2.1. Activity dependence on Au particle size

Based on the characterization results, we have generated a range of Au/anatase and Au/rutile samples with mean Au particle sizes in the range 3.4–10.0 nm. The consequence of variations in Au size and the nature of the support (anatase *vs.* rutile) on the selective hydrogenation of *m*-DNB has been considered. All the Au systems exhibited an essentially time invariant activity and 100% selectivity in terms of $-NO_2$ group reduction with no evidence of hydrodenitrogenation and/or aromatic ring reduction. This is demonstrated by the two representative cases (Au/TiO_2-1 and Au/TiO_2-3) shown in Fig. 6. The combination of stability and selectivity achieved in this study represents a significant development in the application of Au to promote $-NO_2$ group hydrogenation. A decrease in hydrogenation activity with time-on-stream has been reported for reaction over Au/TiO_2 [11,76–78] and linked to active site saturation as a result of strong reactant chemisorption [11,78], metal sintering [76] and coke formation [77]. Deleterious effects due to the generation of water as reaction by-product [79,80], metal leaching [81] and coke formation [82–85] have been suggested as potential causes for the temporal loss of activity in the gas-phase hydrogenation of nitroarenes over supported Pd [79–81,83,85] and Cu [82,84]. Catalytic activity was assessed in terms of nitro-group reduction efficiency by applying pseudo-first order kinetics [25,36,37]

$$\ln\left[\frac{1}{(1-x_{-NO_2})}\right] = k\left(\frac{n_{Au}}{F_{-NO_2}}\right) \tag{6}$$

where F_{-NO_2} is the total inlet molar $-NO_2$ flow rate and n_{Au} represents the number of moles of Au in the catalyst bed; (n_{Au}/F_{-NO_2}) has the physical meaning of contact time. The linear correlation between $\ln(1-(x_{-NO_2}))^{-1}$ and (n_{Au}/F_{-NO_2}) is shown in Fig. 7A, taking Au/TiO_2-1 and Au/TiO_2-3 as representative catalysts. The raw pseudo-first order rate constants (k) for Au/anatase and Au/rutile are given in Table 1 and Table 2, respectively. A direct comparison of the rate constants for catalysts bearing variable Au dispersion is only meaningful in terms of specific activities, *i.e.* per m^2 of exposed metal. The Au metal surface area was estimated from

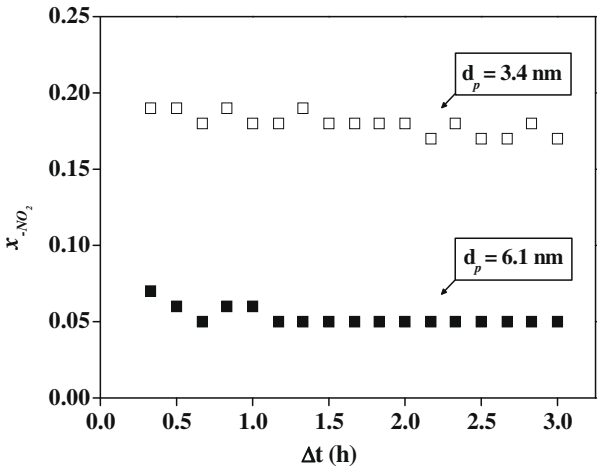

Fig. 6. Variation of $-NO_2$ fractional conversion (x_{-NO_2}) with time-on-stream over (□) Au/TiO_2-1 (Au/$-NO_2 = 2 \times 10^{-3}$ mol_{Au} h $mol^{-1}_{-NO_2}$) and (■) Au/TiO_2-3 (Au/$-NO_2 = 1 \times 10^{-2}$ mol_{Au} h $mol^{-1}_{-NO_2}$) at 473 K.

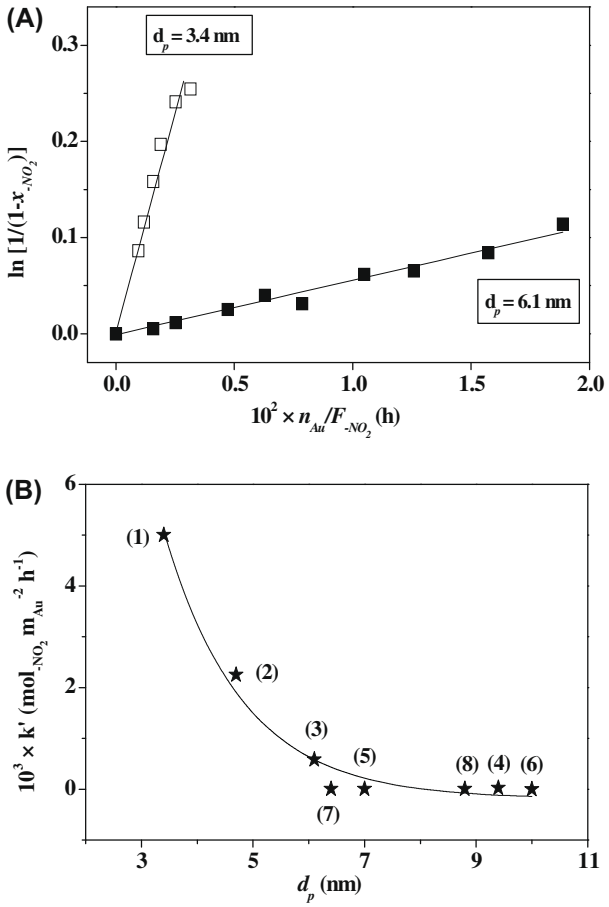

Fig. 7. (A) Pseudo-first-order kinetic plots for reaction over (□) Au/TiO_2-1 and (■) Au/TiO_2-3 at 473 K. (B) Relationship between specific rate constant (k') and Au particle size (d_p) for reaction over Au/TiO_2-1 (1), Au/TiO_2-2 (2), Au/TiO_2-3 (3), Au/TiO_2-4 (4), Au/TiO_2-5 (5), Au/TiO_2-6 (6), Au/TiO_2-7 (7) and Au/TiO_2-8 (8).

$$S_{Au}\ (m_{Au}^2\ g_{Au}^{-1}) = \frac{6}{\rho_{Au} \times d_p} \tag{7}$$

assuming that the metal particles approximate a spherical morphology (consistent with the TEM analysis) where $\rho_{Au} = 18.88\ g\ cm^{-3}$ and d_p is the surface area-weighted mean Au particle size, as measured by TEM (see Tables 1 and 2). The specific pseudo-first order rate constant (k') was then calculated from

$$k'\ (mol_{-NO_2}\ m_{Au}^{-2}\ h^{-1}) = \frac{k\ (mol_{-NO_2}\ g_{Au}^{-1}\ h^{-1})}{S_{Au}\ (m_{Au}^2\ g_{Au}^{-1})} \tag{8}$$

The relationship between specific activity and mean Au particle size for all the catalysts considered in this study is shown in Fig. 7B. The tendency of increasing k' with decreasing d_p is diagnostic of a particle size sensitivity where smaller Au particles (10.0 → 3.4 nm) exhibited an enhanced intrinsic $-NO_2$ hydrogenation efficiency. Furthermore, the results demonstrate that the nature of the support (anatase:rutile ratio) does not impact significantly on hydrogenation rate, which is governed by the Au particle size. A dependence of hydrogenation rate on support for Au on reducible carriers has been reported [78] and ascribed to the formation of electron-rich Au *via* support-metal electron transfer [86], the formation of unselective Au particles with different morphology [87] and/or reactant activation at the Au-support interface [88]. Moreover, Jongsomjit et al. [89] found, for Co/TiO_2, a distinct activity response in the hydrogenation of CO associated with differences in the rutile:anatase ratio. Our results show an equivalent specific $-NO_2$ reduction rate over systems with similar Au particle size but quite different support composition, as illustrated by the data points 3 (Au/TiO_2-3, d_p = 6.1 nm and 20% rutile) and 7 (Au/TiO_2-7, d_p = 6.4 nm and 100% rutile). Moreover, taking an equivalent support composition (18 ± 2% rutile, see data points 1 and 3 in Fig. 7B), the catalyst bearing the smaller Au particles (Au/TiO_2-1, d_p = 3.4 nm) delivered an order of magnitude higher specific rate (when compared with Au/TiO_2-3, d_p = 6.1 nm). Our results find agreement with the published studies suggesting that the presence of nanoscale Au particles (<10 nm) is essential for significant activity [7,8]. Variations in hydrogenation rate for Au particles in the range 3–10 nm have been reported [9,11,90] and linked (in the case of acrolein hydrogenation over Au/TiO_2) to modifications in the electronic character of small Au particles [16]. There have been a limited number of studies dealing with the electronic properties of Au particles on TiO_2 (1 1 0) single crystal surfaces [91–93]. Charge transfer from Au particles to TiO_2 has been observed [91] as evidenced by a positive shift (to higher binding energy) of XPS Au 4f lines for small particles (up to about 4 nm) when compared with those of metallic Au (such as Au (1 1 1) single crystal). The extent of the shift is dependent on the state of TiO_2 prior to Au deposition with reduced surfaces causing more pronounced shifts [92]. Moreover, Au particles grow in 2 dimensions (2D) up to about 3 nm, above which 3D structures are predominantly formed. More importantly, the mean inner potential (defined as the volume average of the electrostatic potential) for Au particles on TiO_2, as followed by electron holography, increases abruptly for sizes below 5 nm [93]. It is instructive to note that the specific activities that we have recorded converge for Au particles >5 nm, and 5 nm represents a critical mean diameter below which there is a marked rate dependence. In a recent study [9], we examined the hydrogenation of *p*-chloronitrobenzene over oxide (Al_2O_3, TiO_2, CeO_2 and Fe_2O_3)-supported Au prepared by impregnation and deposition–precipitation and demonstrated an increase in the specific hydrogenation rate with decreasing Au particle size (from 9 to 3 nm) regardless of the nature of the support. The results generated in this study provide further corroboration of Au particle size effects in $-NO_2$ reduction over supported Au.

3.2.2. Selectivity dependence on Au particle size

The relationship between initial selectivity (S_0) and fractional *m*-DNB conversion ($x_{m\text{-DNB}}$) resulting from reaction over all eight Au/TiO_2 catalysts is shown in Fig. 8. Two distinct trends in terms of product distribution are in evidence for systems where d_p < 5 nm and ⩾5 nm. Reaction over Au/TiO_2 bearing Au particles <5 nm

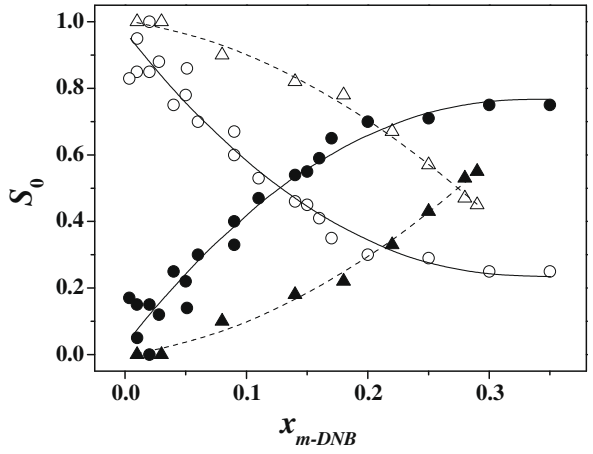

Fig. 8. Variation of *m*-PDM (solid symbols) and *m*-NAN (open symbols) initial selectivity (S_0) with *m*-DNB fractional conversion ($x_{m\text{-DNB}}$) for reaction over catalysts with d_p < 5 nm (▲, Δ) and d_p ⩾ 5 nm (●, ○).

generated *m*-NAN as the preferred product, *i.e.* $S_{m\text{-NAN}} \geqslant 0.5$ at $x_{m\text{-DNB}} \leqslant 0.3$. In contrast, for those catalysts characterized by a mean Au size $\geqslant$5 nm, the formation of *m*-PDM was favoured at $x_{m\text{-DNB}} > 0.10$. This response was independent of support anatase:rutile ratio, and hydrogenation selectivity (in common with activity) was governed by Au particle size. Nitro-group reduction in *m*-DNB can proceed *via* a consecutive and/or parallel mechanism. The two possible pathways are identified in the reaction network shown in Fig. 9. The formation of *m*-PDM can take place *via* a consecutive (Path A, with *m*-NAN as reaction intermediate) and/or a parallel (Path B) concerted mechanism according to:

$$m\text{-DNB} + 3H_2 \xrightarrow{k_1} m\text{-NAN} + 2H_2O \quad (9)$$

$$m\text{-NAN} + 3H_2 \xrightarrow{k_2} m\text{-PDM} + 2H_2O \quad (10)$$

$$m\text{-DNB} + 6H_2 \xrightarrow{k_3} m\text{-PDM} + 4H_2O \quad (11)$$

where, taking the mass balance for each component and applying pseudo-first order kinetics

$$\frac{dN_{m\text{-DNB}}}{d(n_{Au}/F_{m\text{-DNB}})} = -(k_1 + k_3) \times N_{m\text{-DNB}} \quad (12)$$

$$\frac{dN_{m\text{-NAN}}}{d(n_{Au}/F_{m\text{-DNB}})} = k_1 \times N_{m\text{-DNB}} - k_2 \times N_{m\text{-NAN}} \quad (13)$$

$$\frac{dN_{m\text{-PDM}}}{d(n_{Au}/F_{m\text{-DNB}})} = k_2 \times N_{m\text{-NAN}} + k_3 \times N_{m\text{-DNB}} \quad (14)$$

where N_i represents the molar fraction of the *i*th compound and k_j represents the pseudo-first order rate constant of step *j*. Combination of Eqs. (12) and (13) gives

$$\frac{dN_{m\text{-NAN}}}{dN_{m\text{-DNB}}} = -L + M \times \left(\frac{N_{m\text{-NAN}}}{N_{m\text{-DNB}}}\right) \quad (15)$$

with

$$L = \frac{k_1}{k_1 + k_3} \quad \therefore \quad M = \frac{k_2}{k_1 + k_3} \quad (16)$$

which, by formal integration, results in

$$N_{m\text{-NAN}} = \left(\frac{L}{1 - M}\right) \times \left(N_{m\text{-DNB}}^{M} - N_{m\text{-DNB}}\right) \quad (17)$$

and the values of *L* and *M* can be determined by non-linear mathematical fitting. The applicability of this parallel/consecutive mechanism can be assessed from Fig. 10, which reveals a more than adequate representation of the selectivity trends. A predominantly

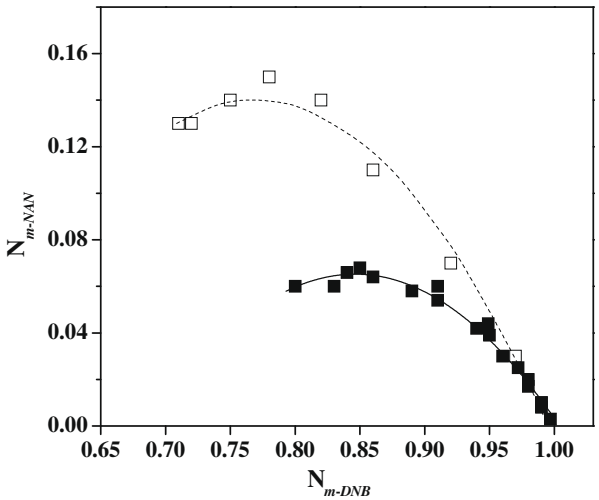

Fig. 10. Dependence of *m*-NAN mole fraction ($N_{m\text{-NAN}}$) on *m*-DNB conversion ($N_{m\text{-DNB}}$) for reaction over catalysts with $d_p < 5$ nm (□) and $d_p \geqslant 5$ nm (■). *Note*: Lines represent fit to the parallel/consecutive model, see Eq. (17).

stepwise –NO_2 group reduction mechanism should result in a value for *L* close to unity, *i.e.* $k_3 \sim 0$. The extracted values of $L = 0.99$ (for $d_p < 5$ nm) and $L = 0.81$ (for $d_p \geqslant 5$ nm) confirm that smaller Au particles promote a predominantly consecutive hydrogenation, resulting in a higher maximum $N_{m\text{-NAN}}$ (see Fig. 10).

We were unable to find any published report that has considered the effect of TiO_2 anatase and/or rutile content on the catalytic action of supported Au. However, we can flag related studies where selectivity in the hydrogenation of acetylene [94] and alkadienes [74] over Pd/TiO_2 showed a dependence on TiO_2 composition, *i.e.* variations in the amount and/or mobility of Ti^{3+} on anatase and rutile. Claus et al. [95] investigated the hydrogenation of crotonaldehyde over Pt/TiO_2 and found a similar selectivity response (to crotyl alcohol) for conversions $\leqslant$50% but proposed an optimum (65% anatase) composition for higher conversions, attributing this to product adsorption/readsorption effects that were dependent on the TiO_2 phase composition. We can tentatively associate our observed selectivity response in terms of Au size to critical differences in the active site electronic structure, which can influence *m*-DNB adsorption/activation. Gold nanoparticle size is known to influence the reactant adsorption and impact on selectivity in hydrogenation reactions [17,96]. The formation of $Au^{\delta+}$ and $Au^{\delta-}$

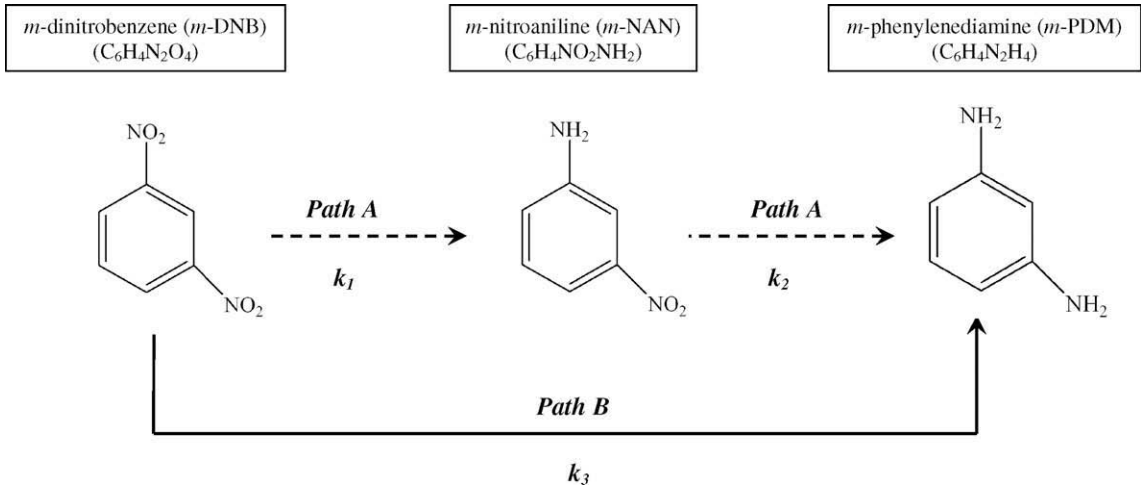

Fig. 9. Reaction pathways associated with the hydrogenation of *m*-dinitrobenzene (*m*-DNB) to *m*-nitroaniline (*m*-NAN) and *m*-phenylenediamine (*m*-PDM).

associated with large (9 nm) and small (3 nm) Au clusters, respectively, on TiO_2 has been demonstrated by EXAFS [97]. Indeed, Zhang et al. [98], studying the hydrogenation of 1,3-butadiene over Au/ZrO_2, ascribed the distinct selectivity response (with respect to butene or butane) to differences in the Au charge. Our results establish for the first time a significant Au particle size effect on the product distribution for the gas-phase hydrogenation of *m*-DNB.

4. Conclusions

The results presented in this study support the following conclusions:

Temperature-programmed reduction of 0.1 and 1 mol% Au-loaded TiO_2 over the temperature range 603–1273 K generated supported Au metal particles with mean diameters in the range 3.4–10.0 nm as confirmed by HRTEM, DRS UV–vis and XRD measurements.

The complete allotropic transition (from anatase to rutile) of the starting TiO_2 support was attained at $T = 1273$ K where the incorporation of Au lowered the temperature requirements by up to 400 K; anatase transformation was promoted to a greater extent at the higher Au loading.

In the gas-phase hydrogenation of *m*-DNB, all Au/TiO_2 catalysts delivered time invariant conversions. The support composition (or anatase:rutile ratio) did not influence the nitro-group reduction rate, which was controlled by Au particle size with increasing specific rates for particles <5 nm: specific rate was insensitive to particle sizes >5 nm.

m-DNB hydrogenation generated *m*-NAN (partial reduction) and/or *m*-PDM (complete reduction) where the reaction proceeded *via* a predominantly stepwise reaction mechanism. *m*-NAN formation was favoured for reaction over Au particles <5 nm. We associate this response with a modification of the electronic character of the Au nanoparticles that impacts on *m*-DNB adsorption/activation mechanism.

Acknowledgments

We are grateful to Dr. W. Zhou and Mr. R. Blackley for their contribution to the TEM analysis. We acknowledge Dr. P. Vaqueiro and M. L. Romero for assistance with the DRS UV–vis measurements. This work was financially supported by EPSRC through Grant 0231 110525. EPSRC support for free access to the TEM/SEM facility at the University of St Andrews is also acknowledged.

References

[1] P.F. Vogt, J.J. Gerulis, Ullmann's Encyclopedia of Industrial Chemistry. "Aromatic Amines", Wiley-VCH Verlag GmbH & Co., KGaA, Weinheim, 2005.
[2] M. Boudart, Adv. Catal. 20 (1969) 153.
[3] S. Chytil, W.R. Glomm, E. Vollebekk, H. Bergem, J. Walmsley, J. Sjöblom, E.A. Blekkan, Micropor. Mesopor. Mater. 86 (2005) 198.
[4] K.V.R. Chary, D. Naresh, V. Vishwanathan, M. Sadakane, W. Ueda, Catal. Commun. 8 (2007) 471.
[5] A. Arcadi, Chem. Rev. 108 (2008) 3266.
[6] J.A. van Bokhoven, J.T. Miller, J. Phys. Chem. C 111 (2007) 9245.
[7] P. Claus, Appl. Catal. A: Gen. 291 (2005) 222.
[8] A.S.K. Hashmi, G.J. Hutchings, Angew. Chem. Int. Ed. 45 (2006) 7896.
[9] F. Cárdenas-Lizana, S. Gómez-Quero, N. Perret, M.A. Keane, Gold Bull. 42 (2009) 38.
[10] J. Jia, K. Haraki, J.N. Kondo, K. Domen, K. Tamaru, J. Phys. Chem. B 104 (2000) 11153.
[11] R. Zanella, C. Louis, S. Giorgio, R. Touroude, J. Catal. 223 (2004) 328.
[12] P.V. Kamat, J. Phys. Chem. C 112 (2008) 18737.
[13] E. Bus, J.T. Miller, J.A. van Bokhoven, J. Phys. Chem. B 109 (2005) 14581.
[14] E. Bus, R. Prins, J.A. van Bokhoven, Catal. Commun. 8 (2007) 1397.
[15] C. Mohr, H. Hofmeister, J. Radnik, P. Claus, J. Am. Chem. Soc. 125 (2003) 1905.
[16] P. Claus, A. Brückner, C. Mohr, H. Hofmeister, J. Am. Chem. Soc. 122 (2000) 11430.
[17] J.E. Bailie, H.A. Abdullah, J.A. Anderson, C.H. Rochester, N.V. Richardson, N. Hodge, J.G. Zhang, A. Burrows, C.J. Kiely, G.J. Hutchings, Phys. Chem. Chem. Phys. 3 (2001) 4113.
[18] I. Dobrosz, K. Jiratova, V. Pitchon, J.M. Rynkowski, J. Mol. Catal. A: Chem. 234 (2005) 187.
[19] F. Moreau, G.C. Bond, A.O. Taylor, J. Catal. 231 (2005) 105.
[20] M. Haruta, Catal. Today 36 (1997) 153.
[21] F. Cárdenas-Lizana, S. Gómez-Quero, A. Hugon, L. Delannoy, C. Louis, M.A. Keane, J. Catal. 262 (2009) 235.
[22] S.H. Overbury, V. Schwartz, D.R. Mullins, W. Yan, S. Dai, J. Catal. 241 (2006) 56.
[23] J. Huang, W.-L. Dai, H. Li, K. Fan, J. Catal. 252 (2007) 69.
[24] T. Akita, P. Lu, S. Ichikawa, K. Tanaka, M. Haruta, Surf. Interface Anal. 31 (2001) 73.
[25] F. Cárdenas-Lizana, S. Gómez-Quero, M.A. Keane, ChemSusChem 1 (2008) 215.
[26] B.K. Min, W.T. Wallace, D.W. Goodman, Surf. Sci. 600 (2006) L7–L11.
[27] K.R. Westerterp, E.J. Molga, K.B. van Gelder, Chem. Eng. Process. 36 (1997) 17.
[28] B. Coq, F. Figuéras, Coord. Chem. Rev. 178–180 (1998) 1753.
[29] G. Zhang, L. Wang, K. Shen, D. Zhao, H.S. Freeman, Chem. Eng. J. 141 (2008) 368.
[30] A. Corma, P. Serna, Science 313 (2006) 332.
[31] N.S. Chaubal, M.R. Sawant, J. Mol. Catal. A: Chem. 261 (2007) 232.
[32] L. Liu, B. Qiao, Y. Ma, J. Zhang, Y. Deng, Dalton Trans. (2008) 2542.
[33] M. Boronat, P. Concepción, A. Corma, S. González, F. Illas, P. Serna, J. Am. Chem. Soc. 129 (2007) 16230.
[34] D. He, H. Shi, Y. Wu, B.-Q. Xu, Green Chem 9 (2007) 849.
[35] Y. Chen, J. Qiu, X. Wang, J. Xiu, J. Catal. 242 (2006) 227.
[36] F. Cárdenas-Lizana, S. Gómez-Quero, M.A. Keane, Catal. Commun. 9 (2008) 475.
[37] F. Cárdenas-Lizana, S. Gómez-Quero, M.A. Keane, Catal. Lett. 127 (2009) 25.
[38] X. Fu, L.A. Clark, Q. Yang, M.A. Anderson, Environ. Sci. Technol. 30 (1996) 647.
[39] G. Tavoularis, M.A. Keane, J. Chem. Technol. Biotechnol. 74 (1999) 60.
[40] G. Yuan, M.A. Keane, Chem. Eng. Sci. 58 (2003) 257.
[41] U. Diebold, Surf. Sci. Rep. 48 (2003) 53.
[42] D.J. Reidy, J.D. Holmes, M.A. Morris, J. Eur. Ceram. Soc. 26 (2006) 1527.
[43] R.I. Bickley, T. Gonzalez-Carreno, J.S. Lees, L. Palmisano, R.J.D. Tilley, J. Solid State Chem. 92 (1991) 178.
[44] T. Sekiya, T. Yagisawa, S. Kurita, J. Ceram. Soc. Jpn. 109 (2001) 672.
[45] M.G. Blanchin, L.A. Bursill, D.J. Smith, Proc. R. Soc. Lond. A 391 (1984) 351.
[46] L.A. Bursill, M.G. Blanchin, D.J. Smith, Proc. R. Soc. Lond. A 391 (1984) 373.
[47] J. Guzman, S. Kuba, J.C. Fierro-Gonzalez, B.C. Gates, Catal. Lett. 95 (2004) 77.
[48] J. Słoczyński, R. Grabowski, A. Kozłowska, P. Olszewski, J. Stoch, J. Skrzypek, M. Lachowska, Appl. Catal. A: Gen. 278 (2004) 11.
[49] S. Gómez-Quero, F. Cárdenas-Lizana, M.A. Keane, Ind. Eng. Chem. Res. 47 (2008) 6841.
[50] B. Hammer, J.K. Nørskov, Nature 376 (1995) 238.
[51] G.C. Bond, D.T. Thompson, Catal. Rev.-Sci. Eng. 41 (1999) 319.
[52] L. Barrio, P. Liu, J.A. Rodríguez, J.M. Campos-Martín, J.L.G. Fierro, J. Chem. Phys. 125 (2006) 164715.
[53] N.S. Phala, G. Klatt, E. van Steen, Chem. Phys. Lett. 395 (2004) 33.
[54] J.-W. Shi, J.-T. Zheng, P. Wu, J. Hazard. Mater. 161 (2009) 416.
[55] R.S. Sonawane, M.K. Dongare, J. Mol. Catal. A: Chem. 243 (2006) 68.
[56] Q. Zhao, M. Li, J. Chu, T. Jiang, H. Yin, Appl. Surf. Sci. 255 (2009) 3773.
[57] B.R. Panda, A. Chattopadhyay, J. Nanosci. Nanotech. 7 (2007) 1911.
[58] X. Hu, D.J. Blackwood, J. Electroceram. 16 (2006) 593.
[59] M. Haruta, CATTECH 6 (2002) 102.
[60] M. Li, W. Hebenstreit, U. Diebold, A.M. Tyryshkin, M.K. Bowman, G.G. Dunham, M.A. Henderson, J. Phys. Chem. B 104 (2000) 4944.
[61] S.-K. Lee, P.K.J. Robertson, A. Mills, D. McStay, N. Elliott, D. McPhail, Appl. Catal. B: Environ. 44 (2003) 173.
[62] G.L. Haller, D.E. Resasco, Adv. Catal. 36 (1989) 173.
[63] S. Díaz-Moreno, D.C. Koningsberger, A. Muñoz-Páez, Nucl. Instrum. Methods Phys. Res. Sect. B 133 (1997) 15.
[64] J. Liu, Microsc. Microanal. 10 (2004) 55.
[65] R. Rodríguez-Talavera, S. Vargas, R. Arroyo-Murillo, R. Montiel-Campos, E. Haro-Poniatowski, J. Mater. Res. 12 (1996) 439.
[66] S. Vargas, R. Arroyo, E. Haro, R. Rodríguez, J. Mater. Res. 14 (1999) 3932.
[67] G. Sankar, K.R. Kannan, C.N.R. Rao, Catal. Lett. 8 (1991) 27.
[68] R.I. Bickley, T. Gonzalez-Carreño, A.R. Gonzalez-Elipé, G. Munuera, L. Palmisano, J. Chem. Soc. Faraday Trans. 90 (1994) 2257.
[69] A.G. Shastri, A.K. Datye, J. Schwank, J. Catal. 87 (1984) 265.
[70] M.A. Debeila, M.C. Raphulu, E. Mokoena, M. Avalos, V. Petranovskii, N.J. Coville, M.S. Scurrell, Mater. Sci. Eng. A 396 (2005) 61.
[71] R. Arroyo, G. Córdoba, J. Padilla, V.H. Lara, Mater. Lett. 54 (2002) 397.
[72] D. Pillay, G.S. Hwang, Phys. Rev. B 72 (2005) 205422.
[73] N. Lopez, J.K. Nørskov, T.V.W. Janssens, A. Carlsson, A. Puig-Molina, B.S. Clausen, J.-D. Grunwaldt, J. Catal. 225 (2004) 86.
[74] Y. Li, B. Xu, Y. Fan, N. Feng, A. Qiu, J.M.J. He, H. Yang, Y. Chen, J. Mol. Catal. A: Chem. 216 (2004) 107.
[75] N. Yao, J. Chen, J. Zhang, J. Zhang, Catal. Commun. 9 (2008) 1510.
[76] T.V. Choudhary, C. Sivadinarayana, A.K. Datye, D. Kumar, D.W. Goodman, Catal. Lett. 86 (2003) 1.
[77] Y. Azizi, C. Petit, V. Pitchon, J. Catal. 256 (2008) 338.
[78] J.A. Lopez-Sanchez, D. Lennon, Appl. Catal. A: Gen. 291 (2005) 230.
[79] P. Sangeetha, P. Seetharamulu, K. Shanthi, S. Narayanan, K.S. Rama Raob, J. Mol. Catal. A: Chem. 273 (2007) 244.

[80] P. Sangeetha, K. Shanthi, K.S.R. Rao, B. Viswanathan, P. Selvam, Appl. Catal. A: Gen. 353 (2009) 160.
[81] K.K. Yeong, A. Gavriilidis, R. Zapf, V. Hessel, Catal. Today 81 (2003) 641.
[82] L. Petrov, K. Kumbilieva, N. Kirkov, Appl. Catal. 59 (1990) 31.
[83] E. Klemm, B. Amon, H. Redlingshöfer, E. Dieterich, G. Emig, Chem. Eng. Sci. 56 (2001) 1347.
[84] S. Diao, W. Qian, G. Luo, F. Wei, Y. Wang, Appl. Catal. A: Gen. 286 (2005) 30.
[85] V. Vishwanathan, V. Jayasri, P.M. Basha, N. Mahata, L.M. Sikhwivhilu, N.J. Coville, Catal. Commun. 9 (2008) 453.
[86] C. Milone, C. Crisafulli, R. Ingoglia, L. Schipilliti, S. Galvagno, Catal. Today 122 (2007) 341.
[87] B.C. Campo, S. Ivanova, C. Gigola, C. Petit, M.A. Volpe, Catal. Today 133–135 (2008) 661.
[88] J.E. Bailie, G.J. Hutchings, Chem. Commun. (1999) 2151.
[89] B. Jongsomjit, T. Wongsalee, P. Praserthdam, Catal. Commun. 6 (2005) 705.
[90] C. Mohr, H. Hofmeister, P. Claus, J. Catal. 213 (2003) 86.
[91] T. Okazawa, M. Fujiwara, T. Nishimura, T. Akita, M. Kohyama, Y. Kido, Surf. Sci. 600 (2006) 1331.
[92] A. Howard, D.N.S. Clark, C.E.J. Mitchell, R.G. Egdell, V.R. Dhanak, Surf. Sci. 518 (2002) 210.
[93] K. Okazaki, S. Ichikawa, Y. Maeda, M. Haruta, M. Kohyama, Appl. Catal. A: Gen. 291 (2005) 45.
[94] J. Panpranot, K. Kontapakdee, P. Praserthdam, J. Phys. Chem. B 110 (2006) 8019.
[95] P. Claus, S. Schimpf, R. Schödel, P. Kraak, W. Mörke, D. Hönicke, Appl. Catal. A: Gen. 165 (1997) 429.
[96] B. Pawelec, A.M. Venezia, V. La Parola, S. Thomas, J.L.G. Fierro, Appl. Catal. A: Gen. 283 (2005) 165.
[97] Y. Izumi, D.M. Obaid, K. Konishi, D. Masih, M. Takagaki, Y. Terada, H. Tanida, T. Uruga, Inorg. Chim. Acta 361 (2008) 1149.
[98] X. Zhang, H. Shi, B.-Q. Xu, Catal. Today 122 (2007) 330.